Electronic Supplementary Information for

A porous carbon membrane with abundant intrinsic carbon defects as an integrated gas-diffusion electrode for CO_2 electroreduction

Shixiong Min,[*a,b,c] Huaiyu Chang,[a,b,c] Huanhuan Tao[a,b,c] and Fang Wang[a,b,c]

[a] *School of Chemistry and Chemical Engineering, North Minzu University, Yinchuan, 750021, P. R. China. E-mail: sxmin@nun.edu.cn*

[b] *Ningxia Key Laboratory of Solar Chemical Conversion Technology, North Minzu University, Yinchuan 750021, P. R. China.*

[c] *Key Laboratory of Chemical Engineering and Technology, State Ethnic Affairs Commission, North Minzu University, Yinchuan, 750021, P. R. China.*

1. Experimental

1.1 Chemicals and materials

Basswood was purchased from Ruiyi Wood Industry Company (China). High-purity CO_2 (99.999%) was purchased from Beijing Hepu Beifen Gas Industry Co., Ltd. A 0.1 M $KHCO_3$ (Sigma-Aldrich, 99.5% metals basis) solution was prepared with ultrapure water (18.2 MΩ cm) obtained from a water purification system (Hitech ECO-S15) and used as the electrolyte.

1.2 Synthesis of highly defective porous carbon membrane (HDPCM) electrodes

Natural basswood was first cut into slices (3.5 cm×1.5 cm×2.0 mm) perpendicularly to its growth direction. The natural wood (NW) slices were then pre-carbonized in a muffle furnace at 260 ℃ for 6 h in air atmosphere and then further carbonized in tube furnace at 1000 ℃ for 6 h with a ramping rate of 5 ℃ min^{-1} under Ar atmosphere (40 mL min^{-1}). Afterward, the obtained porous carbon membrane (PCM) was carefully polished with 2000 grit sand paper, washed with water, ethanol, and acetone under ultrasonication, and finally dried in a vacuum oven at 60 ℃ overnight. The PCM was then etched in a CO_2 flow (40 mL min^{-1}) at 550-800 ℃ for 1-3 h to obtain HDPCM electrodes. In brief, the PCM was first heated in Ar atmosphere (40 mL min^{-1}) to predetermined temperature (550-800 ℃) with a ramping rate of 5 ℃ min^{-1}. Once the temperature reached, the Ar was switched to CO_2 and the etching reaction was allowed to proceed at this temperature for 1-3 h. After the completion of etching reaction, the heating atmosphere was switched back to Ar and the obtained samples was allowed to cool to room temperature under Ar protection. For a comparison, the porous carbon membrane with lower defects (denoted as LDPCM) was obtained by heating PCM in a Ar flow (40 mL min^{-1}) using exactly the same procedure for the preparation of HDPCM.

1.3 Characterization

X-ray diffraction (XRD) patterns were investigated with a Rigaku smartlab diffractometer with a nickel filtrated Cu *K*α radiation in the 2θ range of 5~80° with a scanning rate of 5° min^{-1}. Scanning electron microscopy (SEM) images were taken with a ZEISS EVO 10 scanning electron microscope. Transmission electron microscopy (TEM) images were taken with a FEI Talos F200x field emission transmission electron microscope. X-ray photoelectron spectroscopy (XPS) measurements were performed on a Thermo Fisher Escalab-250Xi electron spectrometer using an Al Kα X-ray source. Binding energies were referenced to the C 1s peak (set at 284.4 eV) of the sp^2 hybridized (C=C) carbon from the sample. Near edge X-ray absorption fine structure (NEXAFS) data were taken in an ultrahigh vacuum chamber with a base pressure of 1×10^{-10} mbar at the Surface, Interface and Nanostructure Science (SINS) beam-line (a soft X-ray facility) located at the Singapore Synchrotron Light Source (SSLS). All spectra were recorded at room temperature (300 K) using the total electron yield (TEY) mode. The photon energy was calibrated using a standard gold sample in the chamber. The specific surface areas of the samples were determined with the Brunauer-Emmett-Teller (BET) equation at 77 K by using an adsorption apparatus (Micromeritics ASAP 2460). Raman spectra were collected using a Raman spectrometer system (HORIBA Scientific LabRAM HR Evolution) using a 532 nm laser as the excitation source. Electron paramagnetic resonance (EPR) spectra were carried out on JEOL FA-200 at room temperature. The contact angles of the electrodes were evaluated on a JGW-360 A goniometer (China). The compression experiment was performed by a single column system (HZ-1003) with a compressed speed of 3 mm min^{-1}.

1.4 Electrocatalytic CO_2 reduction reaction in a H-type cell

The electrocatalytic CO_2 reduction experiments were performed on a custom-made three-electrode system with a gas-tight H-type cell with two compartments. The

cathode and anode compartments were separated with a proton exchange membrane (Nafion 117). A Pt mesh and a saturated Ag/AgCl electrode were used as counter and reference electrodes, respectively. The as-fabricated electrodes (1.0 cm×1.0 cm) were directly soldered to a Cu wire as the working electrode. A 0.1 M $KHCO_3$ aqueous solution was used as the electrolyte. The electrochemical measurements were conducted using a CHI 660E potentiostat (CH Instruments, Inc., Shanghai, China). All of the applied potentials were recorded against Ag/AgCl (saturated KCl) reference electrode and then converted to the reversible hydrogen electrode (RHE) reference scale after iR_s compensation according to E (*vs*. RHE)=E (*vs*. Ag/AgCl)+0.0592×pH-iR_s. The solution resistance (R_s) was determined by potentiostatic electrochemical impedance spectroscopy (EIS) measurements, which were performed in a frequency range from 0.01 Hz to 100 kHz at a voltage amplitude of 5 mV.

The linear sweep voltammetry (LSV) was performed in the potential range of 0 to -0.8 V *vs.* RHE at a scan rate of 0.5 mV s^{-1} in N_2- or CO_2-saturated 0.1 M $KHCO_3$ solution, respectively. Prior to the experiments, CO_2 was firstly purged into the $KHCO_3$ solution for at least 30 min to remove residual air in the cathodic compartment reservoir and ensure continuous CO_2 saturation. The chronoamperometry was performed at each potential for several hours. The gas effluent from the cathodic compartment was connected to the gas sampling loop of an online pre-calibrated gas chromatography (GC, A91 Plus PANNA), which was equipped with a packed HN column and a 5 Å molecular sieve. The gas phase composition was analyzed by A91 Plus every 30 min. High purity N_2 (99.999%) was used as the carrier gas. A thermal conductivity detector (TCD) was used to quantify H_2, while then a flame ionization detector (FID) equipped with a methanizer to quantify CO.

The faradaic efficiency (FE) of the gas products at each applied potential were

calculated by using the volume concentrations detected by the GC as below:

$$FE_i = \frac{2FV_iGtp_0}{RT_0Q_{\text{total}} \times 10^6} \times 100\%$$

where V_i (vol %) is volume concentration of CO or H_2 in the exhaust gas from the electrochemical cell (GC data) at a given sampling time, G (mL min^{-1}) is gas flow rate at room temperature and ambient pressure, t (min) is electrolysis time, p_0 is pressure (1.01×10^5 Pa), R is the gas constant (8.314 J mol^{-1} K^{-1}), T_0 is temperature (298.15 K), Q_{total} (C) is integrated charge passed during electrolysis (Chronoamperometry data), F is the Faradaic constant (96485 C mol^{-1}).

The produced liquid products were quantitatively measured by using the ^{1}H-nuclear magnetic resonance spectroscopy (^{1}H-NMR) with a Bruker (AVANCE III, 500 MHz). Typically, 2 mL of electrolyte was mixed with D_2O (1 mL) and dimethyl sulfoxide (DMSO, 0.5 mL) for NMR analysis.

1.5 Measurements of the electrochemically active surface area (ECSA)[1]

Cyclic voltammetry (CV) tests were performed in CO_2-purged 0.05 M $K_3[Fe(CN)_6]$ solution (0.1 M $KHCO_3$ as supporting electrolyte) to determine the electrochemically active surface areas (ECSAs) of the all samples.[1] In this system, the relationship between the peak current value [$(i_{pc}+i_{pa})/2$] and the square root of the potential scanning velocity ($v^{1/2}$) can be described by the Randles-Sevcik equation:

$$i_p = 2.69 \times 10^5 n^{3/2} A D^{1/2} v^{1/2} C$$

where i_p is the peak current value (A); n is the number of electron transfer; A is the ESCA of the electrode (cm^2); D is the diffusion coefficient (cm^2 s^{-1}); C is the concentration of $K_3[Fe(CN)_6]$ (mol cm^{-3}); v is the scanning speed (V s^{-1}).

1.6 Estimation of active site density and turnover frequency (TOF)

The underpotential deposition (UPD) of copper (Cu) has been used to estimate the

number of active sites for the electrodes.[2,3] Briefly, the electrochemical cleaning of the electrodes was performed in a 0.5 M H_2SO_4+20 mM $CuSO_4$+60 mM NaCl solution at 1.059 V vs. RHE for 180 s, followed by the deposition of Cu at various underpotentials for 120 s in the same solution. A linear voltammetric scan was then performed at 1 mV s^{-1} from the set underpotential to a point at which all the UPD Cu had been removed. The active site number and the corresponding TOF for CO_2 electroreduction to CO can be estimated from the required charges for copper stripping according to the following equations (1) and (2)[4,5], respectively:

$$N_A = \frac{Q_{Cu^{2+}}}{2FS} \quad (1)$$

$$\text{TOF } (h^{-1}) = \frac{j_{CO}}{zFN_A} \times 3600 \quad (2)$$

where N_A (mol cm^{-2}) represents the density of active sites, S (cm^{-2}) is the geometric area of the electrode, $Q_{Cu^{2+}}$ (C) is the required charges for UPD stripping, F is the Faradaic constant (96485 C mol^{-1}), and j_{CO} is the CO partial current density at a certain applied potential (A cm^{-2}).

1.7 Electrocatalytic CO_2 reduction in a flow cell

The as-prepared HDPCM electrode was cut into the desired dimension and directly used as the cathode in a flow cell. To increase the hydrophobicity of HDPCM electrode, a certain amount of polytetrafluoroethylene (PTFE) suspension (15 mg mL^{-1}) was spray-coated on the one side of HDPCM electrode. A Ni foam and a saturated Ag/AgCl were used as the anode and reference electrode, respectively, which were separated by anion exchange membrane (Fumasep-FAA-3-PK-130). A 1.0 M KOH aqueous solution was utilized as the electrolyte and pumped into cathode chamber at a flow rate of 7.5 mL min^{-1}. CO_2 was fed into cathode chamber at a flow rate of 30 mL min^{-1}.

2. Additional data

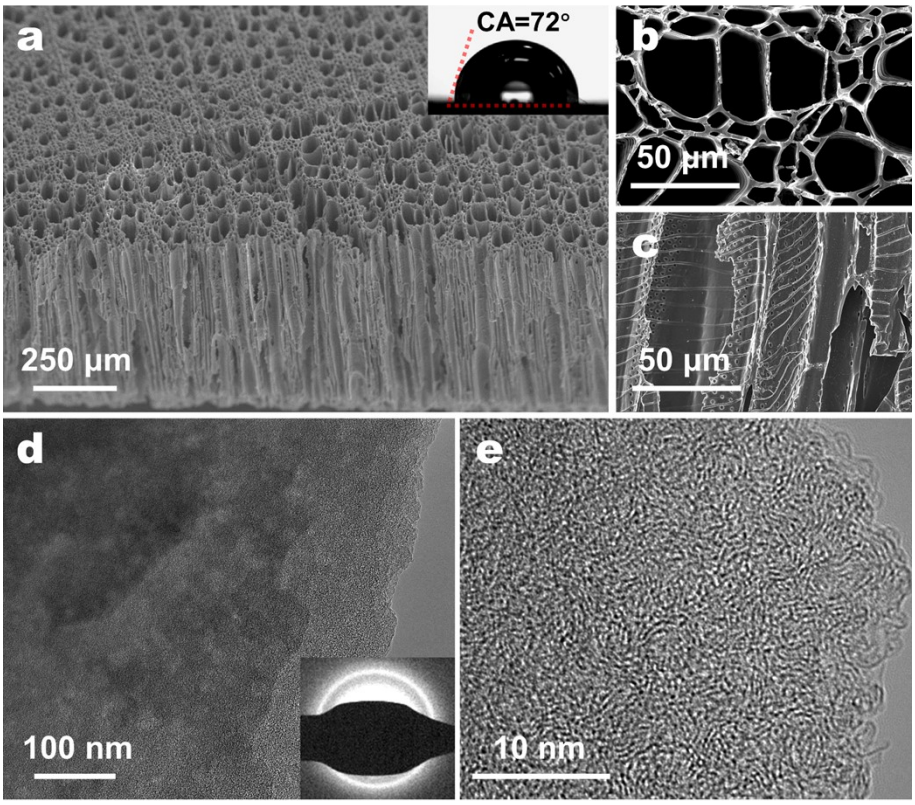

Fig. S1 (a-c) SEM and (d, e) TEM images of the LDPCM electrode. Insets in panel (a) and (d) show the CA and the SAED pattern of the LDPCM electrode.

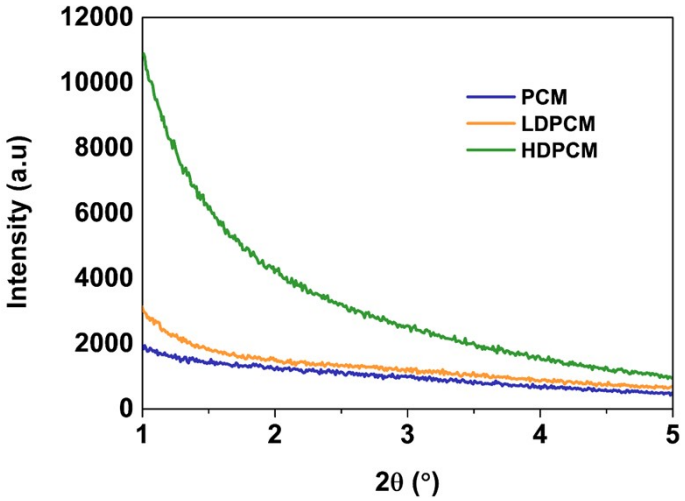

Fig. S2 Small-angle XRD patterns (1~5°) of PCM, LDPCM, and HDPCM electrodes.

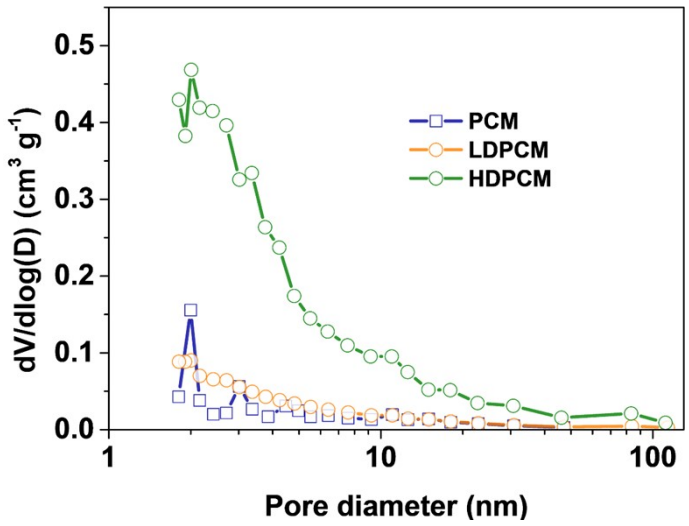

Fig. S3 Pore size distribution curves of PCM, LDPCM, and HDPCM electrodes.

Table S1 Textural properties of PCM, LDPCM, and HDPCM electrodes.

Electrode	S_{BET}(m^2/g)	Pore volume (cm^3/g)	Pore size (nm)
PCM	158.8	0.09	2.35
LDPCM	270.2	0.15	2.24
HDPCM	888.9	0.54	2.42

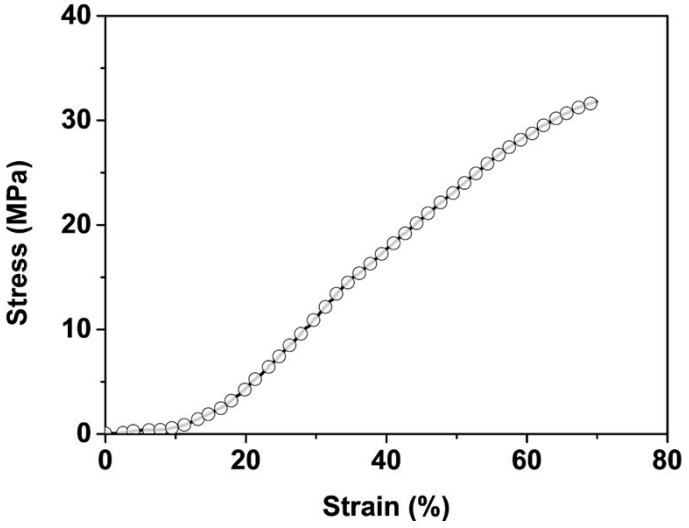

Fig. S4 Stress-strain curve of the as-fabricated HDPCM electrode.

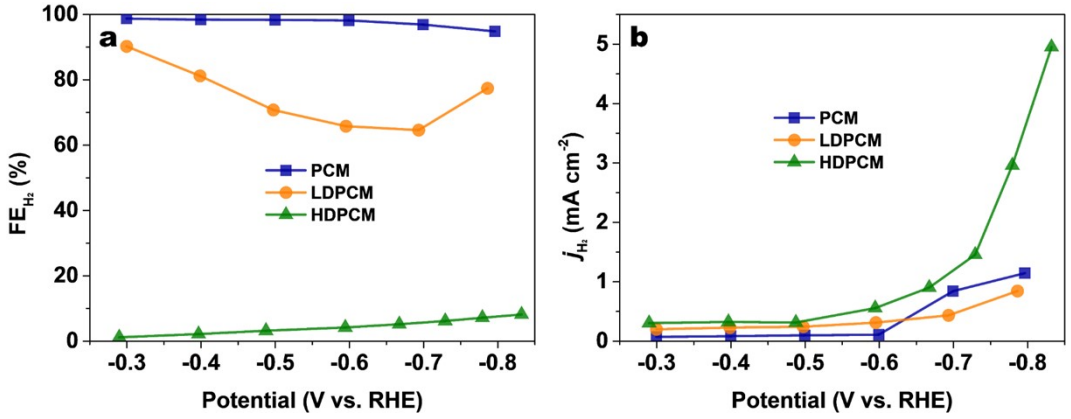

Fig. S5 (a) FE_{H_2} and (b) j_{H_2} values of PCM, LDPCM, and HDPCM electrodes as a function of applied potential.

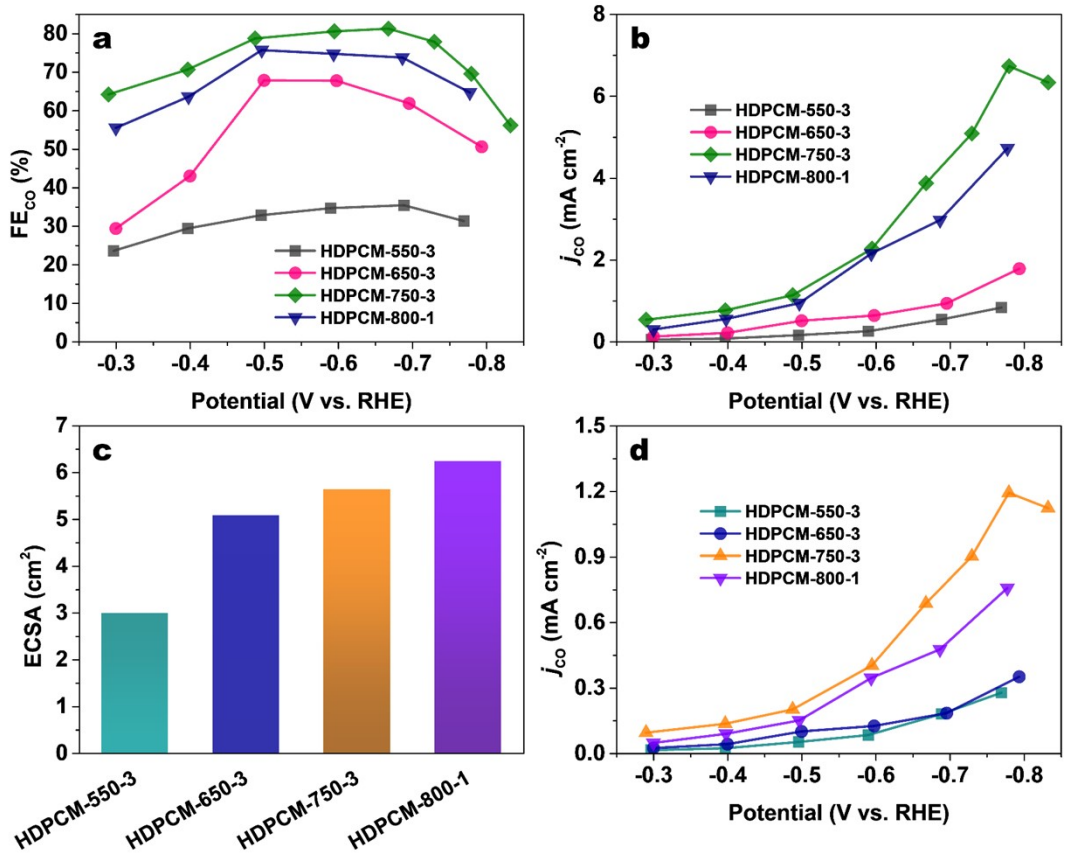

Fig. S6 (a) FE_{CO} and (b) j_{CO} values of the HDPCM electrodes prepared by CO_2 thermal etching at different temperatures plotted against applied potentials. (d) ECSAs of the HDPCM electrodes prepared by CO_2 thermal etching at different temperatures and the corresponding ECSA-normalized j_{CO} values plotted against applied potentials.

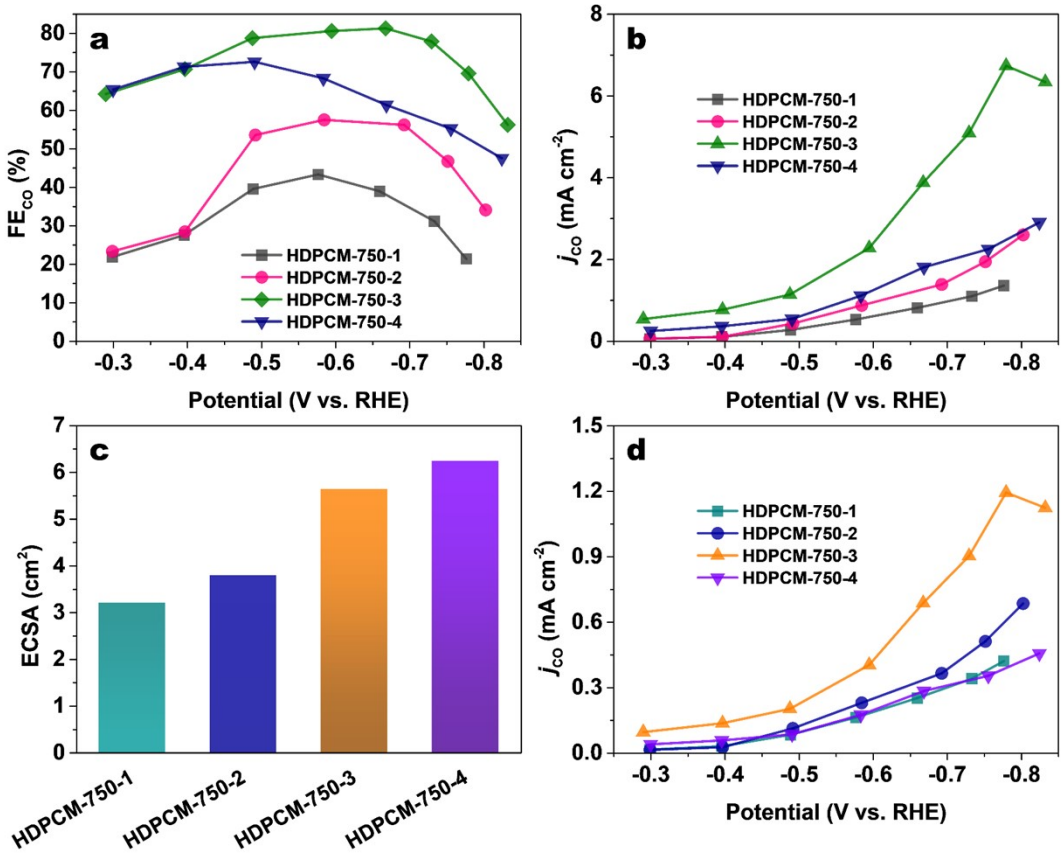

Fig. S7 (a) FE_{CO} and (b) j_{CO} values of the HDPCM electrodes prepared by CO_2 thermal etching at different times plotted against applied potentials. (d) ECSAs of the HDPCM electrodes prepared by CO_2 thermal etching at different times and the corresponding ECSA-normalized j_{CO} values plotted against applied potentials.

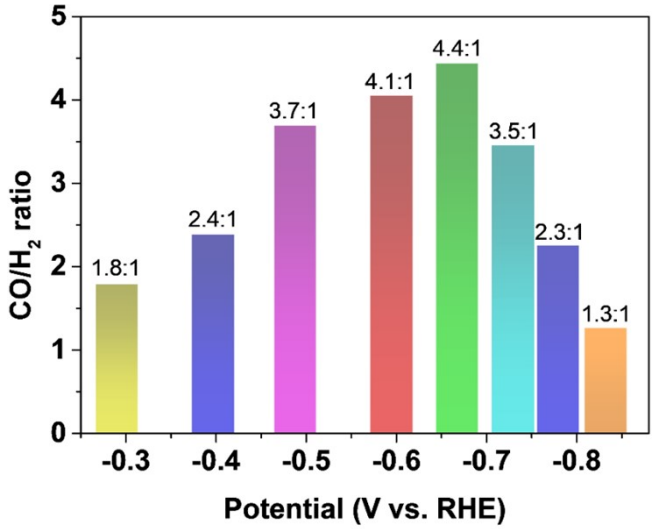

Fig. S8 The calculated CO/H_2 ratios for CO_2RR over HDPCM electrode at various applied potentials.

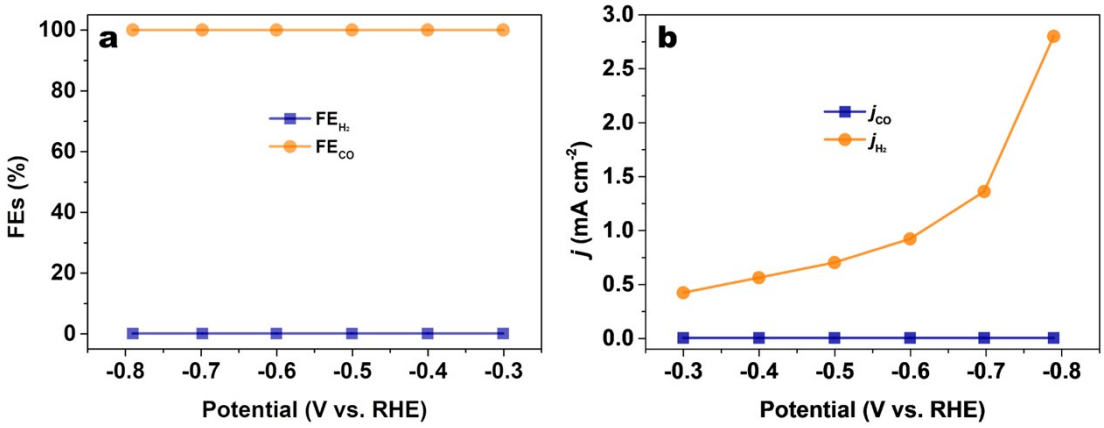

Fig. S9 (a) FEs and (b) current densities for CO and H_2 production on HDPCM electrode in a N_2-saturated 0.1 M $KHCO_3$ solution at various applied potentials.

Table S2 Comparison of CO_2RR performance of our HDPCM electrode with recently reported metal-free carbon electrocatalysts.

Catalysts	Electrolyte ($KHCO_3$)	E (V vs. RHE)	FE_{CO} (%)	j_{CO} (mA cm^{-2})	Ref.
K-defect-C-1100	0.5 M	-0.45	99	~2.5	[6]
NRMC	0.1 M	-0.6	82	2.9	[7]
D-NC-1100	0.1 M	-0.5	~90	~0.7	[8]
DG	0.1 M	-0.6	84	1.3	[9]
DHPC	0.5 M	-0.5	99.5	1.2	[10]
A-350-1000	0.1 M	-1.09	89	~1	[11]
DPC-NH_3-950	0.1 M	-0.6	95.2	2.7	[12]
NCNTs-CAN-850	0.1 M	-1.05	~80	~4	[13]
NCNTs	0.1 M	-0.78	~80	~1	[14]
N-GRW	0.5 M	-0.49	87.6	0.029	[15]
FC	0.1 M	-1.22	93.1	0.394	[16]
NG-800	0.1 M	-0.58	85	~1.8	[17]
NPC-1000	0.5 M	-0.55	98.4	3.01	[18]
F-CPC	0.5 M	-1.0	88.3	27.5	[19]
Pd-NC	0.5 M	-0.5	55	0.244	[20]
P-OLC	0.5 M	-0.9	81	~4.9	[21]
NDD	0.5 M	-1.0	80	~1.0	[22]
N, P-FC	0.5 M	-0.8	83.3	~24	[23]
Co-N_5/HNPCSs	0.2 M	-0.79	99.4	6.2	[24]
Ni/Fe-NC	0.5 M	-0.7	98	9.5	[25]
HDPCM	0.1 M	-0.66 -0.80	81.1 68.1	3.88 6.42	This work

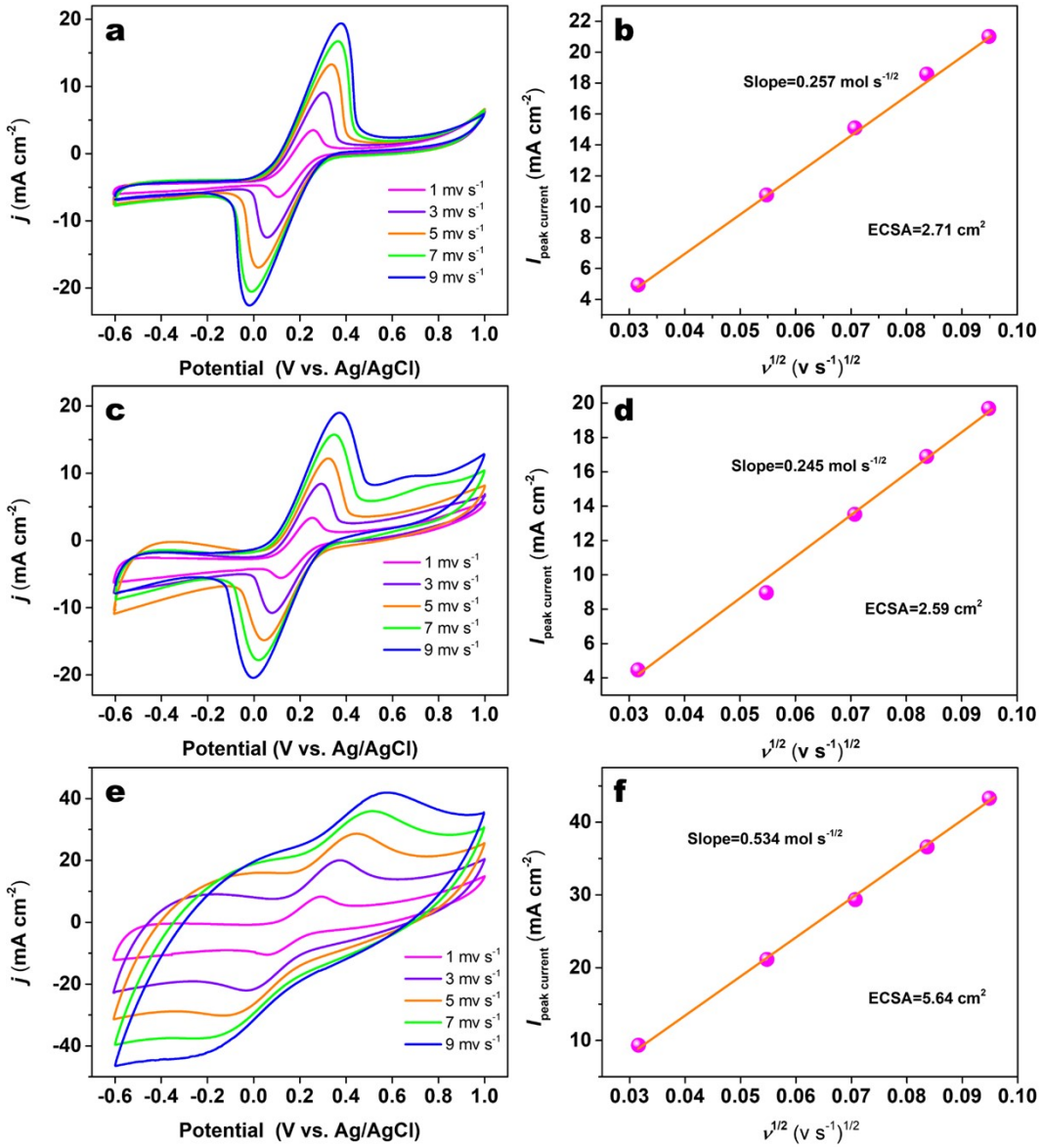

Fig. S10 (a, c, and e) CV curves and (b, d, and f) the corresponding plots of the peak current ((i_{pc}+i_{pa})/2) as a function of square root of the scan rate ($v^{1/2}$) measured in 0.1 M $KHCO_3$ solution containing 0.05 M $K_3[Fe[(CN)_6]$ with (a and b) PCM, (c and d) LDPCM, and (e and f) HDPCM electrodes.

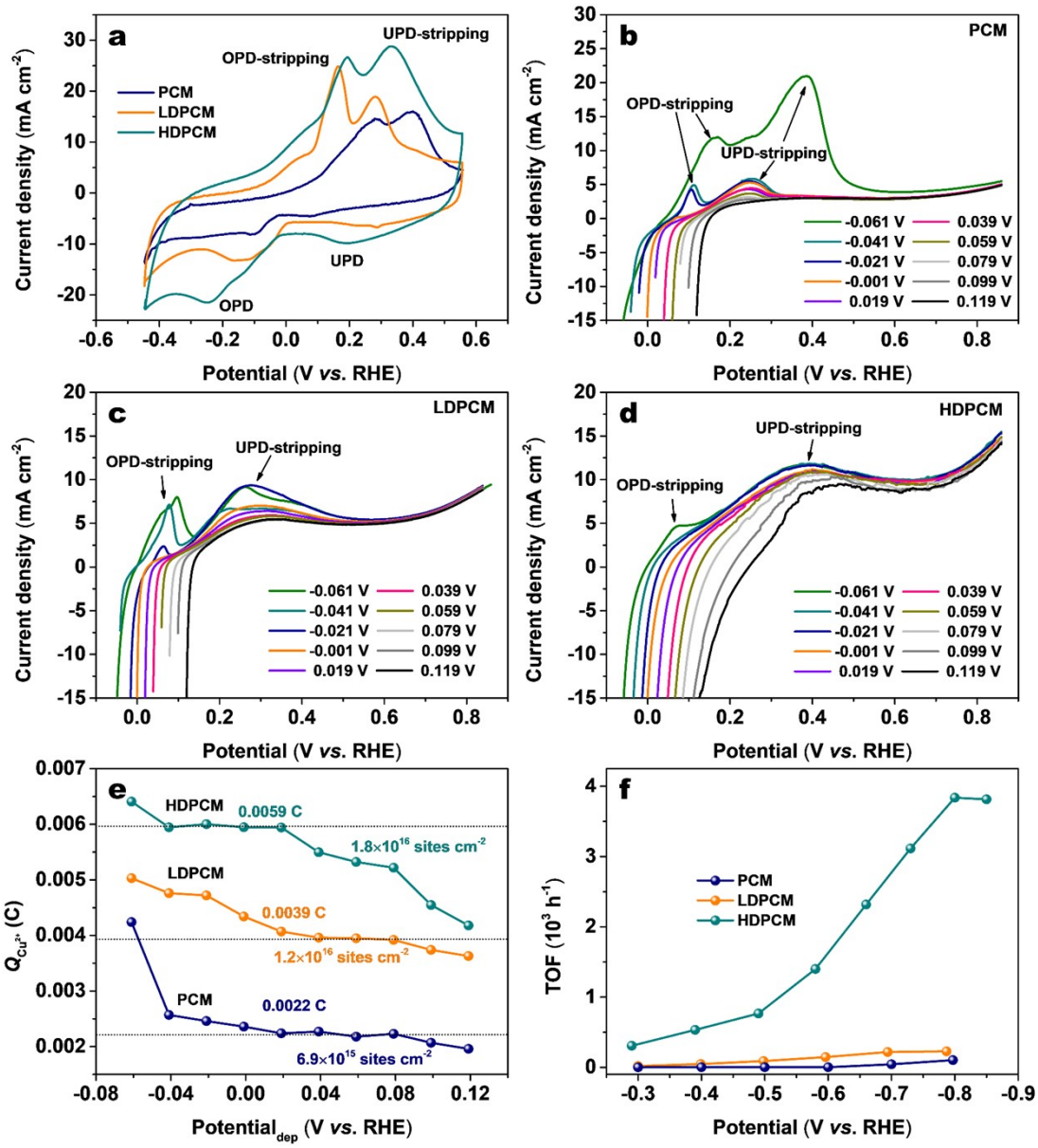

Fig. S11 (a) CV curves for PCM, LDPCM, and HDPCM electrodes in a solution of 0.5 M H_2SO_4+20 mM $CuSO_4$+60 mM NaCl at a scan rate of 1 mV s^{-1}. LSV curves of (b) PCM, (c) LDPCM, and (d) HDPCM electrodes for the stripping of Cu deposited at different overpotentials from -0.061 to 0.119 V vs. RHE in a 0.5 M H_2SO_4+20 mM $CuSO_4$+60 mM NaCl solution (scan rate of 1 mV s^{-1}). (e) The charges required to strip the Cu deposited at different underpotentials for the PCM, LDPCM, and HDPCM electrodes. (f) TOFs of CO production over PCM, LDPCM, and HDPCM electrodes at different applied potentials.

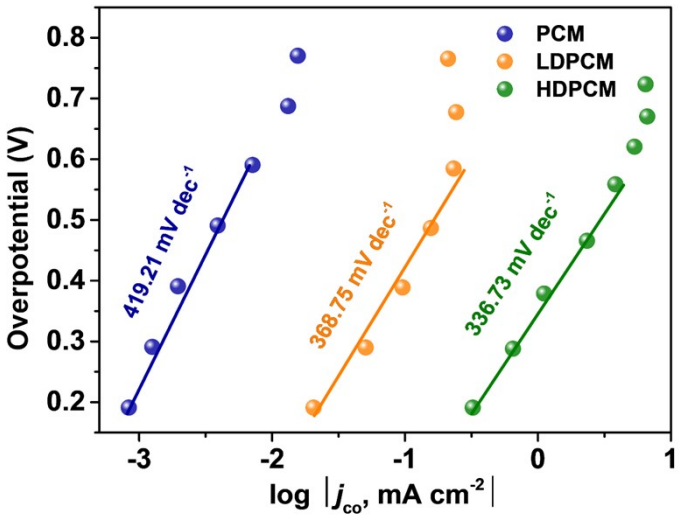

Fig. S12 Tafel plots of CO production for PCM, LDPCM, and HDPCM electrodes.

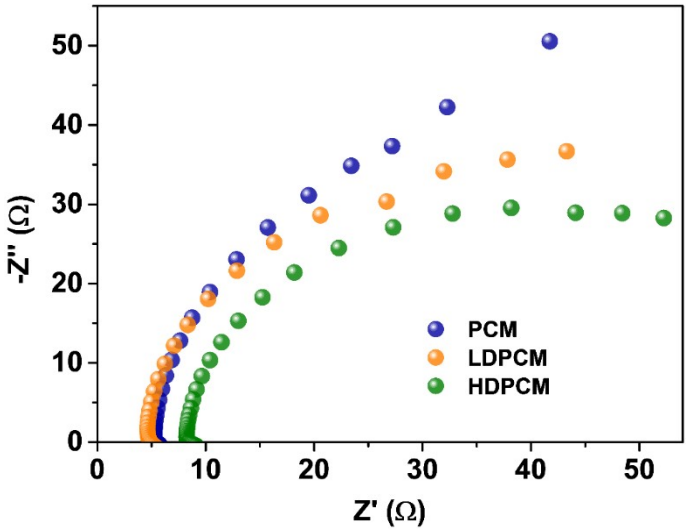

Fig. S13 EIS Nyquist plots of PCM, LDPCM, and HDPCM electrodes measured in CO_2-saturated 0.1 M $KHCO_3$ solutions at -0.3 V *vs*. RHE.

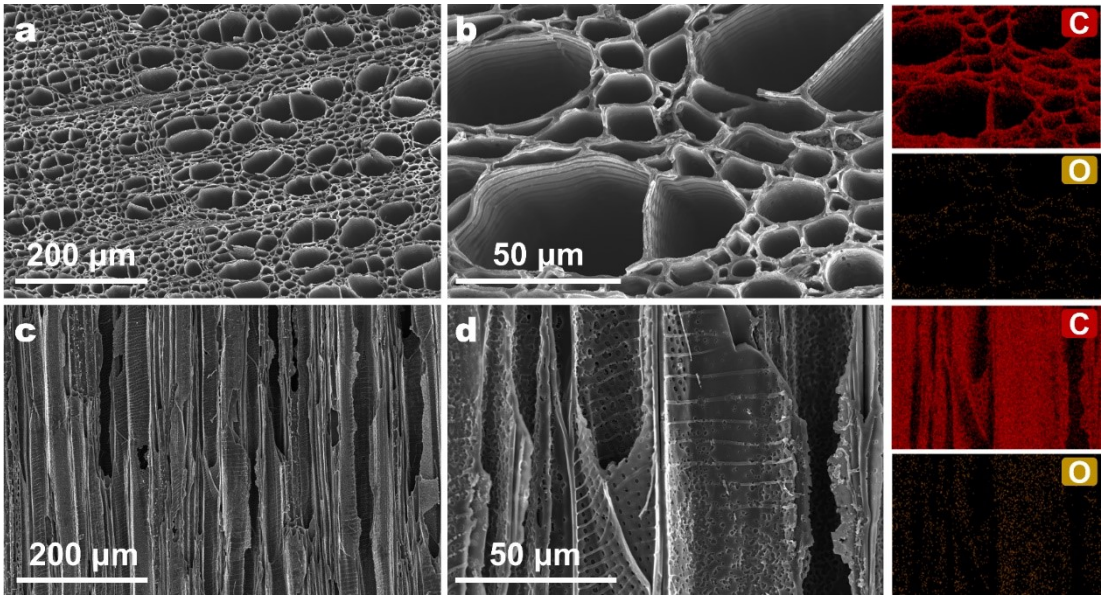

Fig. S14 (a, b) Top-view and (c, d) cross-section SEM images and the corresponding EDX mapping images of the HDPCM electrode after CO_2RR stability test.

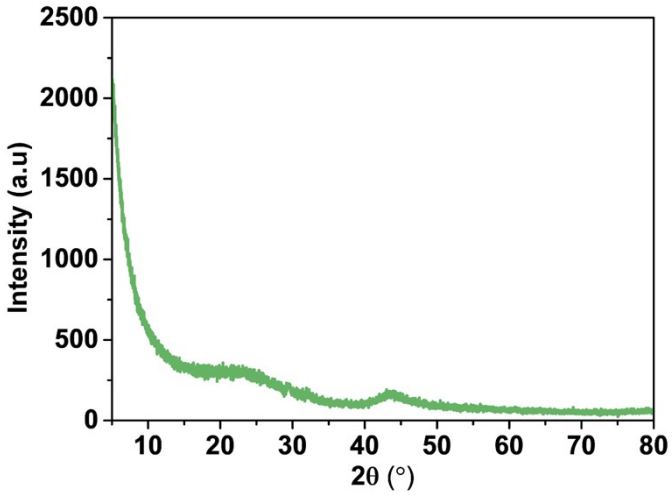

Fig. S15 XRD pattern of the HDPCM electrode after CO_2RR stability test.

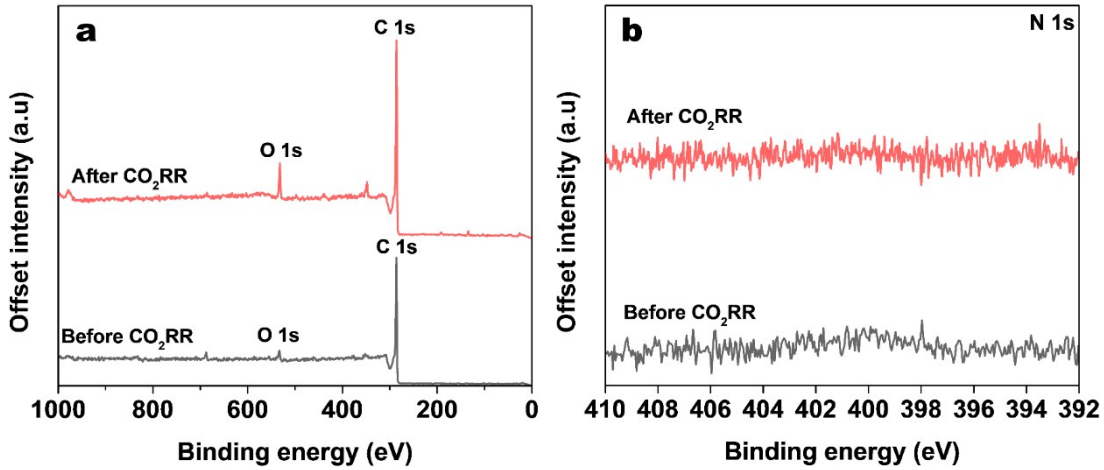

Fig. S16 (a) XPS survey and (b) N 1s XPS spectra of the HDPCM electrode before and after CO_2RR stability test.

References

1. H. Pan, F. Wang, Z. G. Zhang and S. X. Min, *Sustainable Energy Fuels*, 2022, **6**, 2149-2154.
2. C. L. Green and A. Kucernak, *J. Phys. Chem. B*, 2002, **106**, 1036-1047.
3. D. Voiry, H. Yamaguchi, J. Li, R. Silva, D. C. B. Alves, T. Fujita, M. Chen, T. Asefa, V. B. Shenoy, G. Eda and M. Chhowalla, *Nat. Mater.*, 2013, **12**, 850-855.
4. S. Kozuch and J. M. L. Martin, *ACS Catal.*, 2012, **2**, 2787-2794.
5. G. Zhang, T. Wang, M. Zhang, L. Li, D. Cheng, S. Zhen, Y. Wang, J. Qin, Z. J. Zhao and J. Gong, *Nat. Commun.*, 2022, **13**, 7768.
6. L. L. Ling, L. Jiao, X. S. Liu, Y. Dong, W. J. Yang, H. J. Zhang, B. J. Ye, J. Chen and H. L. Jiang, *Adv. Mater.*, 2022, **34**, 2205933.
7. R.H. Daiyan, X. Tan, R. Chen, W. H. Saputera, H. A. Tahini, E. M. Lovell, Y. H. Ng, S. C. Smith, L. M. Dai, X. Y. Lu and R. Amal, *ACS Energy Lett.*, 2018, **3**, 2292-2298.
8. W. Wang, L. Shang, G. J. Chang, C. Y. Yan, R. Shi, Y. X. Zhao, D. J. Yang and T. R. Zhang, *Adv. Mater.*, 2019, **31**, 1808276.

9. P. Han, X. M. Yu, D. Yuan, M. Kuang, Y. F. Wang, A. M. Al-Enizi and G. F. Zheng, *J. Colloid Interface Sci.*, 2019, 534, 332-337.
10. Q. L. Wu, J. Gao, J. R. Feng, Q. Liu, Y. J. Zhou, S. B. Zhang, M. X. Nie, Y. Liu, J. P. Zhao, F. C. Liu, J. Zhong and Z. H. Kang, *J. Mater. Chem. A*, 2020, **8**, 1205-1211.
11. M. J. Chen, S. Wang, H. Y. Zhang, P. Zhang, Z. Q. Tian, M. Lu, X. J. Xie, L. Huang and W. Huang, *Nano Res.,* 2020, **13**, 729-735.
12. Y. Dong, Q. J. Zhang, Z. Q. Tian, B. R. Li, W. S. Yan, S. Wang, K. M. Jiang, J. W. Su, C. W. Oloman, E. L. Gyenge, R. X. Ge, Z. Y. Lu, X. L. Ji and L. Chen, *Adv. Mater.*, 2020, **32**, 2001300.
13. P. P. Sharma, J. Wu, R. M. Yadav, M. Liu, C. J. Wright, C. S. Tiwary, B. I. Yakobson, J. Lou, P. M. Ajayan and X.-D. Zhou, *Angew. Chem. Int. Ed.,* 2015, **127**, 13905-13909.
14. J. Wu, R. M. Yadav, M. Liu, P. P. Sharma, C. S. Tiwary, L. Ma, X. Zou, X. D. Zhou, B. I. Yakobson, J. Lou and P. M. Ajayan*, ACS Nano*, 2015, **9**, 5364-5371.
15. S. Liu, H. Yang, X. Huang, L. Liu, W. Cai, J. Gao, X. Li, T. Zhang, Y. Huang and B. Liu, *Adv. Funct. Mater.,* 2018, **28**, 1-7.
16. J. Xie, X. Zhao, M. Wu, Q. Li, Y. Wang and J. Yao, *Angew. Chem. Int. Ed*., 2018, **57**, 9640-9644.
17. J. Wu, M. Liu, P. P. Sharma, R. M. Yadav, L. Ma, Y. Yang, X. Zou, X. D. Zhou, R. Vajtai, B. I. Yakobson, J. Lou and P. M. Ajayan, *Nano Lett*, 2016, **16**, 466-470.
18. L. Ye, Y. Ying, D. Sun, Z. Zhang, L. Fei, Z. Wen, J. Qiao and H. Huang, *Angew. Chem. Int. Ed*., 2020, **59**, 3244-3251.
19. W. Ni, Y. Xue, X. Zang, C. Li, H. Wang, Z. Yang and Y. M. Yan, *ACS Nano*, 2020, **14**, 2014-2023.

20. Q. He, J. H. Lee, D. Liu, Y. Liu, Z. Lin, Z. Xie, S. Hwang, S. Kattel, L. Song and J. G. Chen, *Adv. Funct. Mater.,* 2020, **30**, e2000407.
21. T. Liu, S. Ali, Z. Lian, C. Si, D. S. Su and B. Li, *J. Mater. Chem. A,* 2018, **6**, 19998-20004.
22. Y. Liu, S. Chen, X. Quan and H. Yu*, J. Am. Chem. Soc.*, 2015, **137**, 11631-11636.
23. X. Xue, H. Yang, T. Yang, P. Yuan, Q. Li, S. Mu, X. Zheng, L. Chi, J. Zhu, Y. Li, J. Zhang and Q. Xu, *J. Mater. Chem. A*, 2019, **7**, 15271-15277.
24. Y. Pan, R. Lin, Y. Chen, S. Liu, W. Zhu, X. Cao, W. Chen, K. Wu, W. C. Cheong, Y. Wang, L. Zheng, J. Luo, Y. Lin, Y. Liu, C. Liu, J. Li, Q. Lu, X. Chen, D. Wang, Q. Peng, C. Chen and Y. Li, *J. Am. Chem. Soc*., 2018, **140**, 4218-4221.
25. W. Ren, X. Tan, W. Yang, C. Jia, S. Xu, K. Wang, S. C. Smith and C. Zhao, *Angew. Chem. Int. Ed.,* 2019, **58**, 6972-6976.